THE ASTROPHYSICAL JOURNAL, 548:919–931, 2001 February 20
© 2001. The American Astronomical Society. All rights reserved. Printed in U.S.A.

DYNAMICAL BAR INSTABILITY IN ROTATING STARS: EFFECT OF GENERAL RELATIVITY

MOTOYUKI SAIJO, MASARU SHIBATA,[1] THOMAS W. BAUMGARTE,[2] AND STUART L. SHAPIRO[3]
Department of Physics, University of Illinois at Urbana-Champaign, Urbana, IL 61801-3080
Received 2000 July 19; accepted 2000 October 11

ABSTRACT

We study the dynamical stability against bar-mode deformation of rapidly and differentially rotating stars in the first post-Newtonian approximation of general relativity. We vary the compaction of the star M/R (where M is the gravitational mass and R the equatorial circumferential radius) between 0.01 and 0.05 to isolate the influence of relativistic gravitation on the instability. For compactions in this moderate range, the critical value of $\beta \equiv T/W$ for the onset of the dynamical instability (where T is the rotational kinetic energy and W the gravitational binding energy) slightly decreases from ~ 0.26 to ~ 0.25 with increasing compaction for our choice of the differential rotational law. Combined with our earlier findings based on simulations in full general relativity for stars with higher compaction, we conclude that relativistic gravitation enhances the dynamical bar-mode instability, i.e., the onset of instability occurs for smaller values of β in relativistic gravity than in Newtonian gravity. We also find that once a triaxial structure forms after the bar-mode perturbation saturates in dynamically unstable stars, the triaxial shape is maintained, at least for several rotational periods. To check the reliability of our numerical integrations, we verify that the general relativistic Kelvin-Helmholtz circulation is well conserved, in addition to rest-mass energy, total mass energy, and linear and angular momentum. Conservation of circulation indicates that our code is not seriously affected by numerical viscosity. We determine the amplitude and frequency of the quasi-periodic gravitational waves emitted during the bar formation process using the quadrupole formula.

Subject headings: gravitation — hydrodynamics — instabilities — relativity — stars: neutron — stars: rotation

1. INTRODUCTION

Stars in nature are usually rotating and subject to nonaxisymmetric rotational instabilities. An exact treatment of these instabilities exists only for incompressible equilibrium fluids in Newtonian gravity (e.g., Chandrasekhar 1969; Tassoul 1978; Shapiro & Teukolsky 1983). For these configurations, global rotational instabilities arise from nonradial toroidal modes $e^{im\varphi}$ ($m = \pm 1, \pm 2, \ldots$) when $\beta \equiv T/W$ exceeds a certain critical value. Here φ is the azimuthal coordinate and T and W are the rotational kinetic and gravitational potential binding energies. In the following we will focus on the $m = \pm 2$ bar mode, since it is the fastest-growing mode when the rotation is sufficiently rapid.

There exist two different mechanisms and corresponding timescales for bar-mode instabilities. Uniformly rotating, incompressible stars in Newtonian theory are secularly unstable to bar-mode formation when $\beta \geq \beta_{\rm sec} \simeq 0.14$. However, this instability can grow only in the presence of some dissipative mechanism, like viscosity or gravitational radiation, and the growth time is determined by the dissipative timescale, which is usually much longer than the dynamical timescale of the system. By contrast, a dynamical instability to bar-mode formation occurs when $\beta \geq \beta_{\rm dyn} \simeq 0.27$. This instability is independent of any dissipative mechanisms, and the growth time is the hydrodynamic timescale of the system.

The secular instability in compressible stars, both uniformly and differentially rotating, has been analyzed numerically within linear perturbation theory, by means of a variational principle and trial functions, by solving the eigenvalue problem, or by other approximate means. These techniques have been applied not only in Newtonian theory (Lynden-Bell & Ostriker 1967; Ostriker & Bodenheimer 1973; Friedman & Schutz 1978; Ipser & Lindblom 1990) but also in a post-Newtonian (PN) framework (Cutler & Lindblom 1992; Shapiro & Zane 1998 for incompressible stars) and in full general relativity (Bonazzola, Frieben, & Gourgoulhon 1996, 1998; Stergioulas & Friedman 1998; Yoshida & Eriguchi 1999). For relativistic stars, the critical value of $\beta_{\rm sec}$ depends on the compaction M/R of the star (where M is the gravitational mass and R the circumferential radius at the equator), on the rotational law and on the dissipative mechanism. The gravitational radiation-driven instability occurs for smaller rotation rates, i.e., for values $\beta_{\rm sec} < 0.14$, in general relativity. For extremely compact stars (Stergioulas & Friedman 1998; Yoshida & Eriguchi 1999) or strongly differentially rotating stars (Imamura et al. 1995), the critical value can be as small as $\beta_{\rm sec} < 0.1$. By contrast, viscosity drives the instability to higher rotation rates $\beta_{\rm sec} > 0.14$ as the configurations become more compact (Bonazzola et al. 1996, 1998; Shapiro & Zane 1998).

Determining the onset of the dynamical bar-mode instability, as well as the subsequent evolution of an unstable star, requires a fully nonlinear hydrodynamic simulation. Simulations performed in Newtonian theory (e.g., Tohline, Durisen, & McCollough 1985; Durisen et al. 1986; Williams & Tohline 1988; Houser, Centrella, & Smith 1994; Smith, Houser, & Centrella 1995; Houser & Centrella 1996; Pickett, Durisen, & Davis 1996; Toman et al. 1998; New, Centrella, & Tohline 2000) have shown that $\beta_{\rm dyn}$ depends only very weakly on the stiffness of the equation of state. Once a bar has developed, the formation of spiral arms

[1] Department of Earth and Space Science, Graduate School of Science, Osaka University, Toyonaka, Osaka 560-0043, Japan.
[2] Fortner Fellow.
[3] Department of Astronomy and NCSA, University of Illinois at Urbana-Champaign, Urbana, IL 61801.

plays an important role in redistributing the angular momentum and forming a core-halo structure. Recently, it has been shown that, similar to the onset of secular instability, $\beta_{\rm dyn}$ can be smaller for stars with a higher degree of differential rotation (Tohline & Hachisu 1990; Pickett et al. 1996).

To date, the dynamical bar-mode instability has been analyzed mainly in Newtonian theory, since until quite recently a stable numerical code capable of performing reliable hydrodynamic simulations in three dimensions plus time in full general relativity has not existed. Some recent developments, however, have advanced the field significantly. New formulations of the Einstein equation based on modifications of the standard (3 + 1) system of equations have resulted in codes which have proved to be remarkably stable over many dynamical timescales (e.g., Shibata & Nakamura 1995; Baumgarte & Shapiro 1999). In addition, gauge conditions which allow long-time stable evolution for rotating, self-gravitating systems and are manageable computationally have been developed (e.g., Shibata 1999b).

The purpose of this paper is twofold. We verify that the point of onset of dynamical bar-mode formation, as measured by β, decreases with increasing compaction, and we furthermore show that in unstable configurations, the bar persists for at least several rotational periods.

In a previous paper Shibata, Baumgarte, & Shapiro (2000) performed simulations of rapidly and differentially rotating neutron stars in full general relativity. They employed the relativistic code of Shibata (1999a) to study the onset and growth of the dynamical bar-mode instability in relativistic stars. They found that for compact stars with $M/R \gtrsim 0.1$, the onset of dynamical instability occurs at $\beta_{\rm dyn} \sim 0.24$–$0.25$, somewhat smaller than the Newtonian value of $\beta_{\rm dyn} \sim 0.26$. In principle, this reduction of $\beta_{\rm dyn}$ could be caused by effects of either general relativity or differential rotation. In order to isolate the two effects one could study sequences of varying compaction M/R or sequences of varying degrees of differential rotation. We choose the former in this paper and focus on the transition to relativistic gravitation as the compaction increases to moderate values.

In fully relativistic evolution codes the Courant condition for the gravitational fields limits the size of the numerical time steps due to the speed of light.[4] As a consequence, the ratio between the dynamical timescale for the matter and the Courant time step for the fields scales approximately as $(M/R)^{-1/2}$, which makes the calculation prohibitively slow for small compactions. In this paper, we therefore adopt the first-order post-Newtonian (1PN) code of Shibata, Baumgarte, & Shapiro (1998) to study the effect of general relativity on $\beta_{\rm dyn}$ for small and moderate compactions. In this formalism, the relativistic evolution equations for the gravitational fields reduce to elliptic equations, which are solved on individual time slices and hence have no Courant condition. The numerical time steps are now limited by the Courant condition for the hydrodynamical evolution equations alone and therefore scale with the dynamical timescale. We evolve models with compactions M/R between 0.01 and 0.05 for several rotational periods to determine their stability. In cases in which a bar forms we also follow the nonlinear growth and saturation of the instability.

Should the star retain its bar-like shape for many rotational periods, then it would emit a quasi-periodic gravitational wave signal. Such a radiator would be potentially a very promising source for the gravitational wave interferometers currently under construction. This prospect has prompted many researchers to study the evolution of the bar-mode instability, most recently New et al. (2000) and Brown (2000). They have performed long-duration Newtonian simulations of dynamically unstable stars that form a bar and then spiral arms. These configurations eject small amounts of mass and then settle down to triaxial stars. For the early stage of the evolution, the results of these two groups are very similar, but for later times some differences arise. According to New et al. (2000), the bar gradually decays after a few rotational periods, probably because of numerical errors associated with the unphysical motion of the center of mass, whereas Brown (2000) reports that the star remains bar-like for more than 10 rotational periods, and presumably until gravitational radiation ultimately drives the decay of the bar.

Given these discrepancies, which are probably a result of numerical inaccuracies, it seems desirable to develop additional criteria to verify the late-time reliability of numerical codes. In particular, it is possible that numerical viscosity associated with finite differencing could lead to an artificial decay of bar modes. In this paper we evaluate the conservation of circulation, which is violated in the presence of viscosity (numerical or otherwise). We present a method for computing the circulation in general relativity and demonstrate that, in our numerical code, the circulation is well conserved.

This paper is organized as follows. In § 2 we present the basic equations of our 1PN formulation of general relativity and describe our initial data in § 3. We discuss our numerical results in § 4, focusing on the dynamical stability of differentially rotating stars. In § 5 we demonstrate the conservation of circulation in our simulations and discuss the emitted gravitational wave signal in § 6. In § 7 we briefly summarize our findings. Throughout this paper, we use the geometrized units with $G = c = 1$ and adopt Cartesian coordinates (x, y, z) with the coordinate time t. Greek and Latin indices take (t, x, y, z) and (x, y, z), respectively.

2. BASIC EQUATIONS

In this section, we briefly review the 1PN formalism of Shibata et al. (1998). We solve the fully relativistic equations of hydrodynamics, but neglect some higher order PN terms in the Einstein field equations.

2.1. *The Field Equations*

Define the spatial projection tensor $\gamma^{\mu\nu} \equiv g^{\mu\nu} + n^\mu n^\nu$, where $g^{\mu\nu}$ is the spacetime metric, $n^\mu = (1/\alpha, -\beta^i/\alpha)$ is the unit normal to a spatial hypersurface, and α and β^i are the lapse function and shift vector. Within a 1PN approximation, the spatial metric $g_{ij} = \gamma_{ij}$ may always be chosen to be conformally flat:

$$\gamma_{ij} = \psi^4 \delta_{ij} , \tag{1}$$

where ψ is the conformal factor (see Chandrasekhar 1965; Blanchet, Damour, & Schäfer 1989). The spacetime line

[4] This limitation could in principle be avoided by using an implicit finite-difference scheme. However, such schemes are more complicated than explicit schemes, and have not yet been implemented for fully relativistic hydrodynamics in three spatial dimensions.

element then reduces to

$$ds^2 = (-\alpha^2 + \beta_k \beta^k)dt^2 + 2\beta_i dx^i dt + \psi^4 \delta_{ij} dx^i dx^j . \quad (2)$$

We adopt maximal slicing, for which the trace of the extrinsic curvature K_{ij} vanishes,

$$K \equiv \gamma^{ij} K_{ij} = 0 . \quad (3)$$

The 1PN field equations for the five unknowns ψ, α, and β^i can then be derived conveniently from the $(3+1)$ formalism.

Since the spatial metric is conformally flat, the transverse part of its time derivative vanishes. The transverse part of the evolution equation of the spatial metric therefore relates the extrinsic curvature to the shift vector,

$$2\alpha\psi^{-4} K_{ij} = \delta_{jl}\partial_i \beta^l + \delta_{il}\partial_j \beta^l - \tfrac{2}{3}\delta_{ij}\partial_l \beta^l . \quad (4)$$

Inserting equation (4) into the momentum constraint equation then yields an equation for the shift vector β^i,

$$\delta_{il}\Delta\beta^l + \frac{1}{3}\partial_i \partial_l \beta^l = 16\pi\alpha J_i + \left[\partial_j \ln\left(\frac{\alpha}{\psi^6}\right)\right] \times \left(\partial_i \beta^j + \delta_{il}\delta^{jk}\partial_k \beta^l - \frac{2}{3}\delta_i^j \partial_l \beta^l\right), \quad (5)$$

where $\Delta \equiv \delta^{ij}\partial_i \partial_j$ is the flat space Laplacian and $J_i \equiv -n^\mu \gamma_i^\nu T_{\mu\nu}$ is the momentum density. In the definition of J_i, $T_{\mu\nu}$ is the stress energy tensor.

The conformal factor ψ is determined from the Hamiltonian constraint

$$\Delta\psi = -2\pi\psi^5 \rho_{\rm H} - \tfrac{1}{8}\psi^5 K_{ij} K^{ij} , \quad (6)$$

where $\rho_{\rm H} \equiv n^\mu n^\nu T_{\mu\nu}$ is the mass-energy density measured by a normal observer.

Maximal slicing implies $\partial_t K = 0$, so that the trace of the evolution equation for the intrinsic curvature yields an equation for the lapse function α,

$$\Delta(\alpha\psi) = 2\pi\alpha\psi^5(\rho_{\rm H} + 2S) + \tfrac{7}{8}\alpha\psi^5 K_{ij} K^{ij} , \quad (7)$$

where $S = \gamma_{jk} T^{jk}$. We also use equation (6) to derive this equation.

Equations (5)–(7) determine the fully nonlinear relativistic metric for maximal slicing within the conformal flatness approximation. None of these equations involve time derivatives, so that in a numerical finite-difference implementation the Courant condition is no longer coupled to the speed of light. Since the conformal flatness approximation introduces errors at higher order than 1PN, it is reasonable to neglect terms in these equations which are also higher than 1PN order. In particular, we discard $\{\partial_j[\ln(\alpha/\psi^6)]\}(\partial_i \beta^j + \delta_{il}\delta^{jk}\partial_k \beta^l - 2\delta_i^j \partial_l \beta^l/3)$ in equation (5), $\psi^5 K_{ij} K^{ij}/8$ in equation (6), and $7\alpha\psi^5 K_{ij} K^{ij}/8$ in equation (7). With these simplifications, the source terms on the left-hand sides of equations (5)–(7) become compact. As a consequence, we can solve these equations numerically very accurately with outer boundary conditions set at fairly small distances outside the matter, and hence on fairly small numerical grids.

The equation for the shift,

$$\delta_{il}\Delta\beta^l + \tfrac{1}{3}\partial_i \partial_l \beta^l = 16\pi\alpha J_i , \quad (8)$$

can be further simplified by introducing a vector B_i and a scalar χ according to

$$\Delta B_i = 4\pi\alpha J_i , \quad (9)$$

$$\Delta\chi = -4\pi\alpha J_i x^i . \quad (10)$$

The shift can then be computed from

$$\delta_{ij}\beta^j = 4B_i - \tfrac{1}{2}[\partial_i \chi + \partial_i(B_k x^k)] , \quad (11)$$

and will automatically satisfy equation (8). The vector-type Poisson equation (eq. [8]) for β^i has hence been reduced to four scalar-type Poisson equations for B_i and χ.

To summarize, we have reduced Einstein equations in a 1PN formalism to six elliptic equations for the six variables $(\alpha\psi, \psi, B_i, \chi)$,

$$\Delta(\alpha\psi) = 2\pi\alpha\psi^5(\rho_{\rm H} + 2S) \equiv 4\pi S_{\alpha\psi} , \quad (12)$$

$$\Delta\psi = -2\pi\psi^5 \rho_{\rm H} \equiv 4\pi S_\psi , \quad (13)$$

$$\Delta B_i = 4\pi\alpha J_i , \quad (14)$$

$$\Delta\chi = -4\pi\alpha J_i x^i . \quad (15)$$

These Poisson-type equations are solved imposing the following boundary condition at outer boundaries

$$\alpha\psi = 1 - \frac{1}{r}\int S_{\alpha\psi} d^3x + O(r^{-3}) , \quad (16)$$

$$\psi = 1 - \frac{1}{r}\int S_\psi d^3x + O(r^{-3}) , \quad (17)$$

$$B_x = -\frac{x}{r^3}\int \alpha J_x x d^3x - \frac{y}{r^3}\int \alpha J_x y d^3x + O(r^{-4}) , \quad (18)$$

$$B_y = -\frac{x}{r^3}\int \alpha J_y x d^3x - \frac{y}{r^3}\int \alpha J_y y d^3x + O(r^{-4}) , \quad (19)$$

$$B_z = -\frac{z}{r^3}\int \alpha J_z z d^3x + O(r^{-4}) , \quad (20)$$

$$\chi = \frac{1}{r}\int \alpha J_i x^i d^3x + O(r^{-3}) . \quad (21)$$

2.2. *The Matter Equations*

For a perfect fluid, the energy momentum tensor takes the form

$$T^{\mu\nu} = \rho\left(1 + \varepsilon + \frac{P}{\rho}\right)u^\mu u^\nu + P g^{\mu\nu} , \quad (22)$$

where ρ is the comoving rest-mass density, ε the specific internal energy, P the pressure, and u^μ the four-velocity.

We adopt a Γ-law equation of state in the form

$$P = (\Gamma - 1)\rho\varepsilon , \quad (23)$$

where Γ is the adiabatic index, which we set to be 2 in this paper.

In the absence of thermal dissipation, equation (23), together with the first law of thermodynamics, implies a polytropic equation of state,

$$P = \kappa\rho^{1+1/n} , \quad (24)$$

where $n = 1/(\Gamma - 1)$ is the polytropic index and κ is a constant. Thus, if the matter satisfies a polytropic equation of state initially, the polytropic form of the equation of state is preserved during the subsequent evolution in the absence of shocks.

TABLE 1

DIFFERENTIALLY ROTATING STARS IN EQUILIBRIUM

Model	r_p/r_e	$\bar{\rho}_{\max}$	$\bar{P}_c$	$\bar{P}_e$	$\bar{M}$	$\bar{M}_0$	$\bar{J}$	T/W	R/M	Stability
I(*a*).....	0.250	0.0117	37.40	83.52	0.113	0.123	0.0264	0.265	20.01	Unstable
I(*b*).....	0.275	0.0125	36.03	80.50	0.110	0.120	0.0245	0.259	19.94	Unstable
I(*c*).....	0.300	0.0135	34.97	78.27	0.107	0.116	0.0221	0.249	20.00	Unstable
I(*d*).....	0.325	0.0148	33.96	75.97	0.109	0.103	0.0198	0.238	20.01	Stable
II(*a*).....	0.250	0.00655	52.39	111.6	0.0711	0.0746	0.0128	0.271	34.34	Unstable
II(*b*).....	0.275	0.00753	50.21	107.1	0.0700	0.0735	0.0120	0.263	34.04	Unstable
II(*c*).....	0.300	0.00821	47.19	100.9	0.0709	0.0746	0.0116	0.252	32.37	Stable
II(*d*).....	0.325	0.00901	46.19	98.48	0.0675	0.0710	0.0102	0.240	32.75	Stable
III(*a*).....	0.250	0.00359	72.64	150.6	0.0417	0.0428	0.00566	0.273	61.36	Unstable
III(*b*).....	0.275	0.00381	70.78	146.7	0.0401	0.0412	0.00511	0.265	62.46	Unstable
III(*c*).....	0.300	0.00430	67.95	140.4	0.0393	0.0404	0.00470	0.254	61.73	Stable
III(*d*).....	0.325	0.00480	66.15	137.1	0.0377	0.0388	0.00417	0.241	61.76	Stable
IV(*a*).....	0.250	0.00218	94.58	193.1	0.0262	0.0266	0.00279	0.275	100.1	Unstable
IV(*b*).....	0.275	0.00236	91.39	186.6	0.0256	0.0260	0.00258	0.267	100.2	Unstable
IV(*c*).....	0.300	0.00265	88.21	180.7	0.0248	0.0251	0.00232	0.255	100.4	Stable
IV(*d*).....	0.325	0.00296	85.81	174.6	0.0238	0.0242	0.00207	0.242	100.1	Stable

NOTE.—$\bar{\rho}_{\max}$: maximum rest-mass density; $\bar{P}_c$: rotational period along the rotational axis; $\bar{P}_e$: rotational period at the equator; $\bar{M}$: gravitational mass; $\bar{M}_0$: rest mass; $\bar{J}$: angular momentum; T: rotational kinetic energy; W: gravitational binding energy; R: equatorial circumferential radius.

From $\nabla_\mu T^{\mu\nu} = 0$ together with the equation of state (eq. [23]), we can derive the energy and Euler equations according to

$$\frac{\partial e_*}{\partial t} + \frac{\partial (e_* v^j)}{\partial x^j} = 0 , \tag{25}$$

$$\frac{\partial (\rho_* \tilde{u}_i)}{\partial t} + \frac{\partial (\rho_* \tilde{u}_i v^j)}{\partial x^j} = -\alpha \psi^6 P_{,i} - \rho_* \alpha \tilde{u}^t \alpha_{,i} + \rho_* \tilde{u}_j \beta^j{}_{,i} + \frac{2\rho_* \tilde{u}_k \tilde{u}_k}{\psi^5 \tilde{u}^t} \psi_{,i} , \tag{26}$$

where

$$e_* = (\rho\varepsilon)^{1/\Gamma} \alpha u^t \psi^6 , \tag{27}$$

$$v^i = \frac{dx^i}{dt} = \frac{u^i}{u^t} , \tag{28}$$

$$\rho_* = \rho \alpha u^t \psi^6 , \tag{29}$$

$$\tilde{u}^t = (1 + \Gamma\varepsilon) u^t , \tag{30}$$

$$\tilde{u}_i = (1 + \Gamma\varepsilon) u_i . \tag{31}$$

Note that we treat the matter fully relativistically; the 1PN approximation only enters through simplifications in the coupling to the gravitational fields. Note also that we do not need to include an artificial viscosity, since we do not encounter any shocks in the simulations in this paper. As a consequence we also do not need to solve the continuity equation

$$\frac{\partial \rho_*}{\partial t} + \frac{\partial (\rho_* v^i)}{\partial x^i} = 0 , \tag{32}$$

since in the absence of shocks it is equivalent to equation (25).

The gravitational mass M (e.g., Bowen & York 1980), rest mass M_0, proper mass M_p, angular momentum J, kinetic energy T, and gravitational binding energy W of a rotating star can be computed from

$$M = -\frac{1}{2\pi} \oint_\infty \nabla^i \psi \, dS_i = \int [(\rho + \rho\varepsilon + P)(\alpha u^t)^2 - P] \psi^5 \, d^3x , \tag{33}$$

$$M_0 \equiv \int \rho u^t \sqrt{-g} \, d^3x = \int \rho_* \, d^3x , \tag{34}$$

$$M_p = \int \rho u^t (1 + \epsilon) \sqrt{-g} \, d^3x = \int \rho_* (1 + \varepsilon) d^3x , \tag{35}$$

$$J = \int T^t_\phi \sqrt{-g} \, d^3x = \int (x J_y - y J_x) \psi^6 d^3x , \tag{36}$$

$$T = \frac{1}{2} \int \Omega T^t_\phi \sqrt{-g} \, d^3x = \frac{1}{2} \int \Omega (x J_y - y J_x) \psi^6 \, d^3x , \tag{37}$$

$$W = M_p + T - M . \tag{38}$$

We also define the quadrupole moments I_{ij} as

$$I_{ij} = \int \rho_* \, x^i x^j \, d^3x , \tag{39}$$

and the nondimensional, scale-invariant ratio $\beta \equiv T/W$, which is very useful to characterize the dynamical stability against bar-mode deformation.

Since we use a polytropic equation of state, it is convenient to rescale all quantities with respect to κ. Since $\kappa^{n/2}$ has dimensions of length, we introduce the following nondimensional variables

$$\begin{aligned} &\bar{t} = \kappa^{-n/2} t, \quad \bar{\tau} = \kappa^{-n/2} \tau, \quad \bar{x} = \kappa^{-n/2} x, \\ &\bar{y} = \kappa^{-n/2} y, \quad \bar{z} = \kappa^{-n/2} z, \quad \bar{\Omega} = \kappa^{n/2} \Omega, \\ &\bar{M} = \kappa^{-n/2} M, \quad \bar{R} = \kappa^{-n/2} R, \quad \bar{C} = \kappa^{-n/2} C, \end{aligned} \tag{40}$$

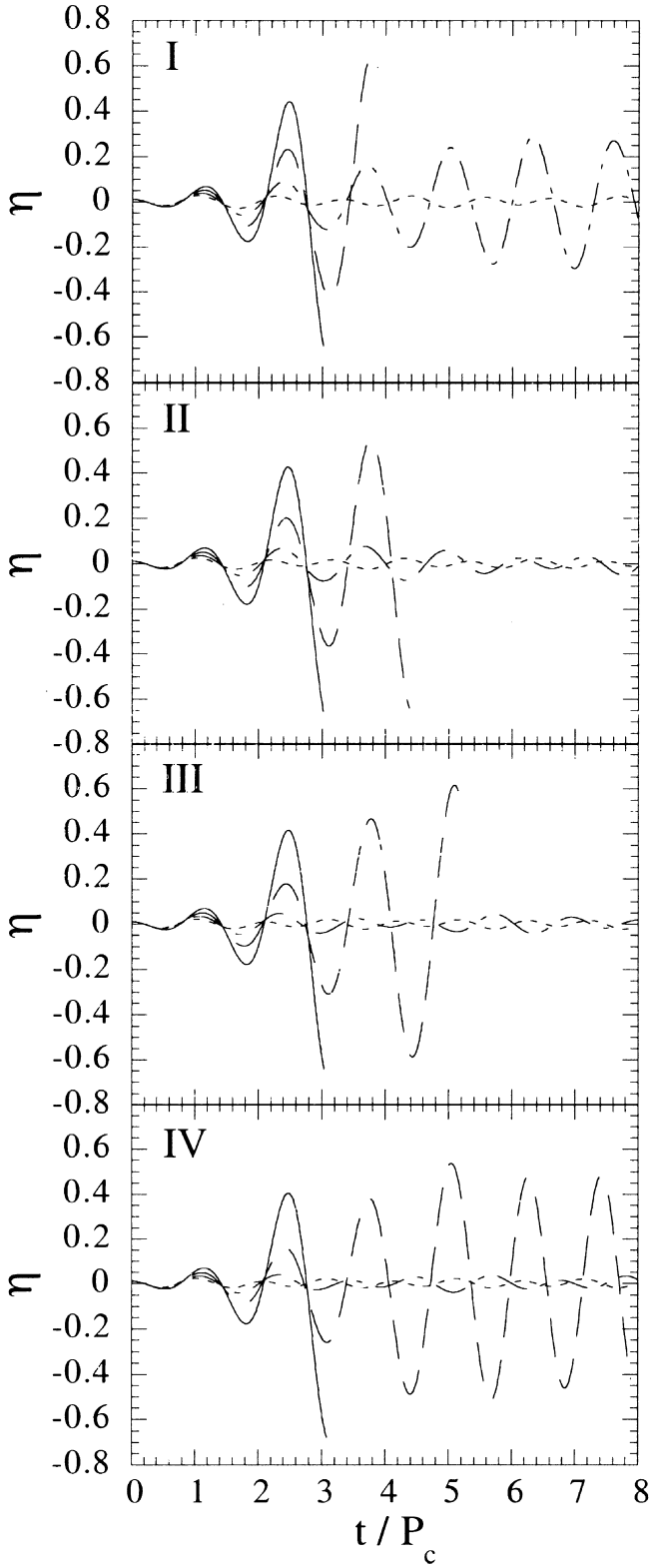

FIG. 1.—Deformation parameter η as a function of t/P_c for our 16 different models (see Table 1). Solid, dashed, dash-dotted and dotted lines denote models (*a*), (*b*), (*c*), and (*d*), respectively. We terminate the simulations after $t \sim 8P_c$, or when 1% of the total rest mass has escaped from the computational grid (models I[*a*], I[*b*], II[*a*], II[*b*], III[*a*], and IV[*a*]).

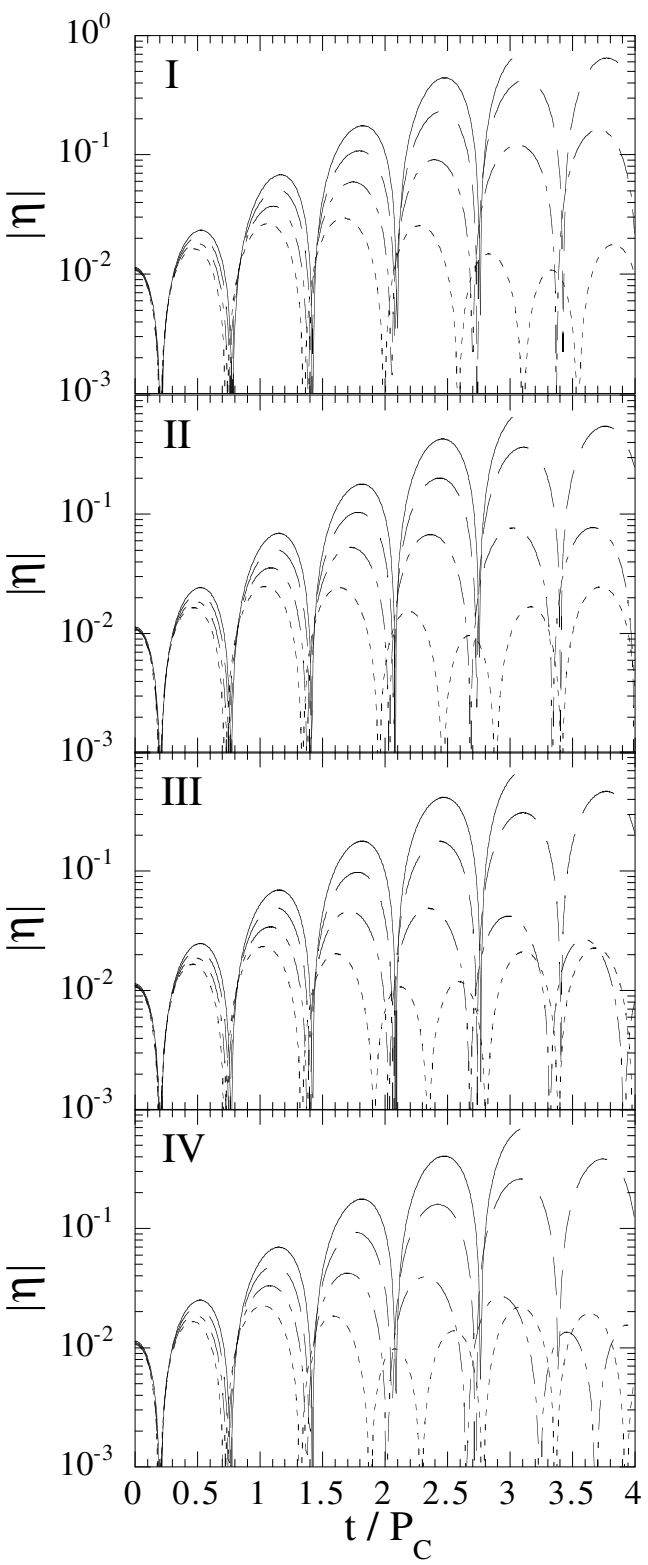

FIG. 2.—Same as Fig. 1, but we show $|\eta|$ on a logarithmic scale for $t/P_c \leq 4$.

where τ is the proper time, Ω the angular velocity of the star, and C circulation (see § 5 for a definition). We also define the central rotation period as $P_c = 2\pi/\Omega_0$. Henceforth, we adopt nondimensional quantities, but omit the bars for convenience (equivalently, we set $\kappa = 1$).

3. INITIAL DATA

To prepare initial data, we construct axisymmetric rotating stars in equilibrium and slightly perturb them. The equilibrium configurations are obtained by solving the equation of hydrostatic equilibrium together with the field equations for metric (i.e., eqs. [12]–[15]). For stationary solutions, the

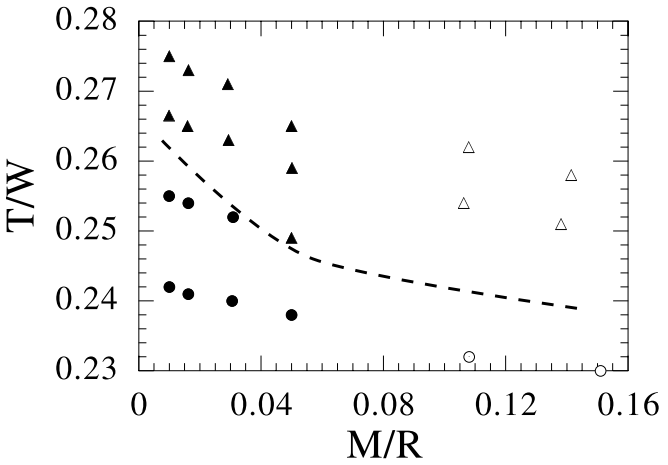

FIG. 3.—Summary of our dynamical stability analysis. All our models are plotted in a β vs. M/R plane, with stable stars denoted by a circle and unstable stars by a triangle. The solid circles and triangles are the models studied in this paper; the open circles and triangles are the models explored in full general relativity by Shibata et al. (2000). We conclude that the critical value of $\beta = \beta_{\rm dyn}$ slightly decreases with increasing compaction M/R. This trend is emphasized by the dotted line, which shows $\beta_{\rm dyn}$ as a function of M/R approximately.

1PN Euler equation can be integrated to yield the 1PN Bernoulli equation

$$\ln(1 + \Gamma\varepsilon) + \tfrac{1}{2}\ln[\alpha^2 - \psi^4\varpi^2(\Omega + \beta^\varphi)^2] + \int u^t u_\varphi \, d\Omega = \text{const} , \tag{41}$$

where $\varpi = (x^2 + y^2)^{1/2}$ and $\beta^\varphi = (x\beta^y - y\beta^x)/\varpi^2$.

Following previous studies (Komatsu, Eriguchi, & Hachisu 1989a, 1989b; Cook, Shapiro, & Teukolsky 1992, 1994; Bonazzola et al. 1993; Salgado et al. 1994; Shibata et al. 2000), we adopt the differential rotation law

$$F(\Omega) \equiv u^t u_\varphi = A^2(\Omega_0 - \Omega) , \tag{42}$$

where A is a constant with dimension of length and Ω_0 is the angular velocity on the rotational axis. With this choice, the hydrostatic equation (eq. [41]) can be integrated analytically. In the Newtonian limit ($u^t \to 1$ and $u_\varphi \to \varpi^2\Omega$) the corresponding rotational profile reduces to

$$\Omega = \frac{A^2\Omega_0}{\varpi^2 + A^2} . \tag{43}$$

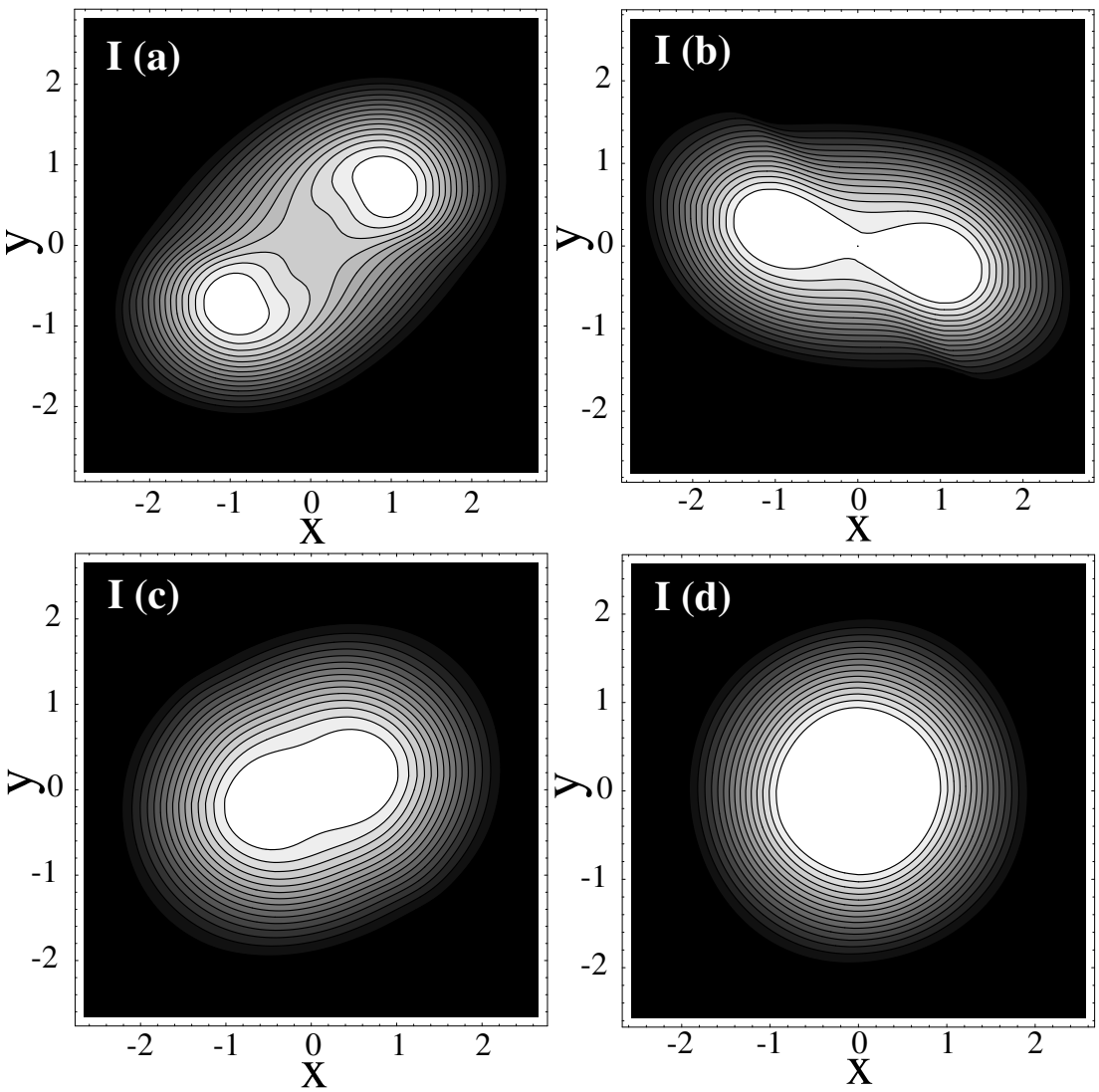

FIG. 4.—Final density contours for ρ_* in the equatorial plane for models I. The contour lines denote densities $\rho_* = 1.3i \times 10^{-3}$ ($i = 1, \ldots, 15$) and at times (*a*) $t/P_c = 2.72$, (*b*) $t/P_c = 3.66$, (*c*) $t/P_c = 7.77$, and (*d*) $t/P_c = 8.16$.

This equation implies that A determines the length scale over which Ω changes, so that a smaller value of A yields a larger degree of differential rotation. As in Shibata et al. (2000), we choose $A = r_e$, where r_e is the equatorial coordinate radius of the star, which corresponds to a moderate degree of differential rotation. This choice allows us to compare directly with the results of Shibata et al. (2000) and to focus on the effects of general relativity. Note that only uniformly rotating stars with sufficiently stiff equations of state ($n \lesssim 0.5$) become dynamically unstable to bar formation before reaching the mass shedding limit, so that the effects of general relativity on $\beta_{\rm dyn}$ have to be studied for differentially rotating stars for typical configurations.

We prepare initial conditions for various values of the compaction M/R and rotation rate. The latter is conveniently parameterized by the deformation r_p/r_e, where r_p is the polar coordinate radius. Since we adopt a 1PN approximation all results are correct only up to the linear order in GM/c^2R (or $[v/c]^2$ where v is a typical speed), implying that we can expect reliable results only for moderate compactions $M/R \ll O(1)$. We therefore restrict our analysis to compactions in the range between 0.01 and 0.05. In Shibata et al. (2000), we found that fully relativistic stars with $M/R \sim 0.10$–0.15 and $A = r_e$ become dynamically unstable against bar-mode formation when $\beta \gtrsim 0.25$. Taking this result as a guide, we prepare rotating stars with $\beta \sim 0.25$, for which the corresponding deformation r_p/r_e takes values ~ 0.25–0.33. We label different initial data models with a Roman number and a Latin letter, e.g., model II(c), where the Roman number labels the compaction, and the Latin letter the deformation, hence β. We tabulate the physical parameters of our initial-value models in Table 1.

In order to trigger bar-mode formation in unstable models, we slightly perturb the density of the equilibrium models according to

$$\rho = \rho^{(\rm equilibrium)}\left[1 + 0.1\left(\frac{x^2 - y^2}{r_e^2}\right)\right]. \tag{44}$$

This perturbation affects only the I_{xx} and I_{yy} components of the quadrupole moment, which changes by approximately 1%. This perturbation can therefore be considered linear initially.

Both for the construction of initial data and their subsequent evolution, we assume planar symmetry across the equator, and solve the equations on a uniform grid of typical size $101 \times 101 \times 51$. In the axisymmetric initial configuration, the star's major and minor axes are covered by 40 and 10–13 grid points. Dynamically unstable stars with high values of β form bars and eject mass. To avoid significant mass outflow across the outer boundaries during the simulation, we use a larger grid of $141 \times 141 \times 71$ grid points for these models. We terminate any simulation when 1% of the total rest mass has been ejected from the numerical grid or the evolution time reaches around $8P_c$. Our longest runs took about 18,000 time steps, and consumed about 80 CPU hours on a VX/4R vector-parallel computer at the National Astronomical Observatory of Japan.

4. DYNAMICAL STABILITY OF DIFFERENTIALLY ROTATING STARS

We evaluate the stability of the perturbed rotating stars by monitoring the distortion parameter

$$\eta \equiv \frac{I_{xx} - I_{yy}}{I_{xx} + I_{yy}}, \tag{45}$$

which is a measure of the magnitude of the bar-mode perturbation. In Figure 1, we show η as a function of time for all our models. When the star is dynamically unstable, η grows exponentially up to a saturation level at which $\eta = O(1)$. Once the perturbation has saturated, the maximum value of η remains nearly constant on dynamical timescales, implying that the bar structure persists. For stable stars, the maximum value of $\eta \ll 1$ remains approximately constant throughout the evolution.

The early exponential growth in unstable stars can be seen more clearly in Figure 2, where we plot $|\eta|$ as a function of time on a logarithmic scale. We can determine the growth time τ_g and the oscillation period τ_o by fitting to a function

$$\eta = \eta_0\, 10^{t/\tau_g} \cos\,(2\pi t/\tau_o + \varphi_0), \tag{46}$$

where η_0 and φ_0 are constants. We tabulate τ_g and τ_o for the unstable stars in Table 2. Interestingly, τ_o depends only very weakly on M/R and β, which agrees with the fully relativistic findings of Shibata et al. (2000).

Stable stars may show signs of an exponential growth very early on, but their distortion parameter always remains very small, $\eta \ll O(1)$. As a criterion for stability, we therefore check whether η follows an exponential growth as in equation (46) up to large values $\eta = O(1)$. Judging from this criterion, models I(a), I(b), I(c), II(a), II(b), III(a), III(b), and IV(a), and IV(b) are dynamically unstable. We summarize these results in Figure 3, where we denote stable and unstable models in a M/R versus β plane. The critical value $\beta_{\rm dyn}$ approaches ~ 0.26 in the Newtonian limit $M/R \to 0$, and decreases to ~ 0.25 for $M/R = 0.05$. Our Newtonian value differs slightly from the result for uniformly rotating, incompressible stars ($\beta = 0.27$), which is most likely a result of the differential rotation in our models. Our results confirm the fully relativistic results of Shibata et al. (2000), which we have also included in Figure 3. There we showed that $\beta_{\rm dyn}$ decreases to $\lesssim 0.24$ for large compactions, $M/R \gtrsim 0.1$.

In Figures 4, 5, 6, and 7, we show contours of the density ρ_* in the equatorial plane for the final stages of the dynamical evolution. These plots clearly exhibit a triaxial structure for the unstable models, while for stable models the density distribution hardly changes during the evolution.

TABLE 2

τ_o AND τ_g IN THE EARLY STAGE OF BAR FORMATION

Model	τ_o/P_c	τ_g/P_c
I(a)	1.30	1.54
I(b)	1.31	2.17
I(c)	1.29	3.52
II(a)	1.30	1.57
II(b)	1.31	2.30
III(a)	1.31	1.60
III(b)	1.31	2.45
IV(a)	1.30	1.61
IV(b)	1.30	2.63

NOTE.—τ_o: oscillation period of bar-mode perturbation. τ_g: growth time of bar-mode perturbation (see eq. [46]).

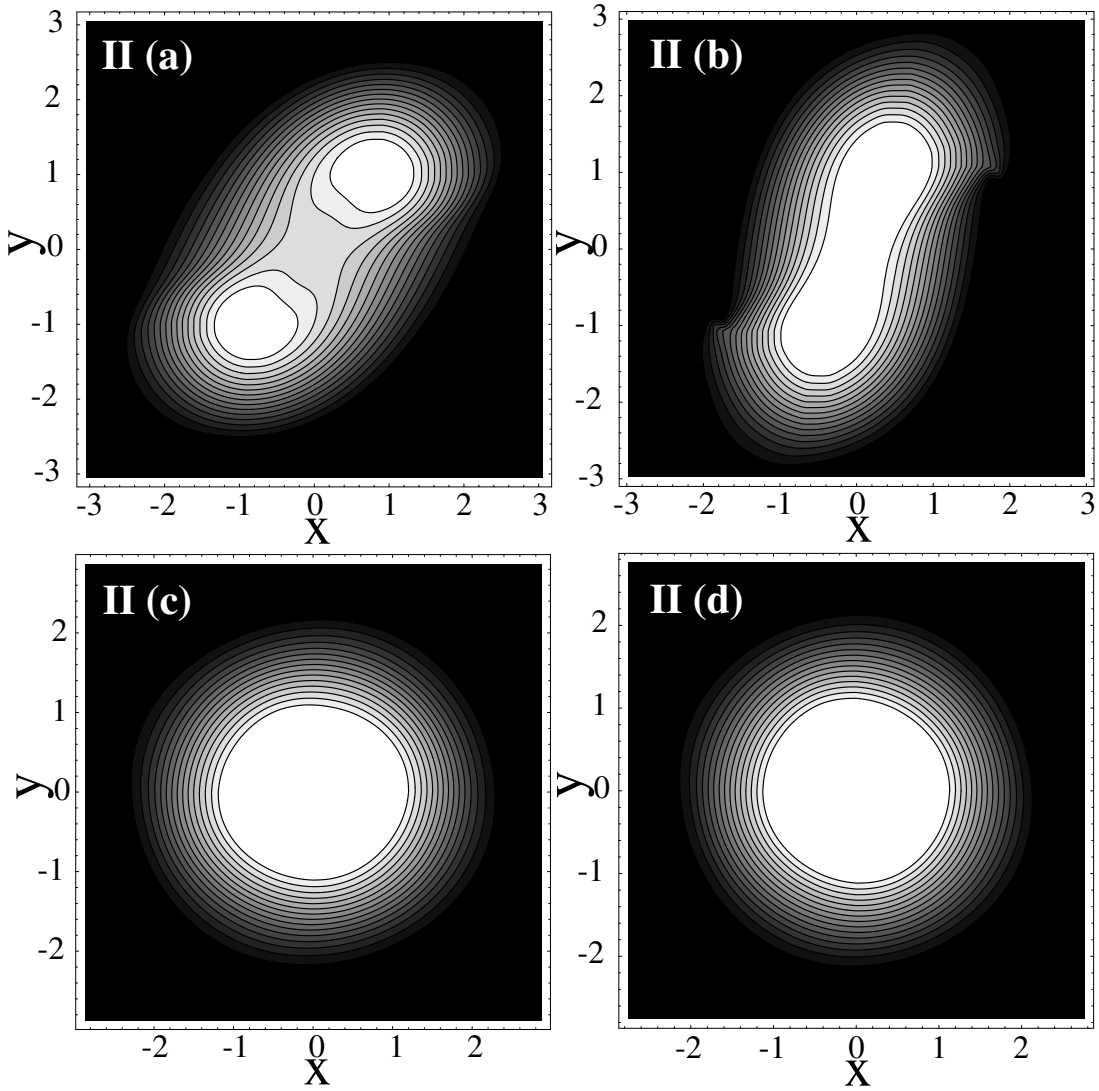

FIG. 5.—Same as Fig. 4, for models II. The contour lines denote densities $\rho_* = 6.0i \times 10^{-4}$ ($i = 1, \ldots, 15$) at times (*a*) $t/P_c = 2.80$, (*b*) $t/P_c = 4.27$, (*c*) $t/P_c = 8.38$, and (*d*) $t/P_c = 8.25$.

Once the bars in dynamically unstable models have saturated, they persist with very little change for several rotation periods (see, e.g., models I[*c*] and IV[*b*] in Fig. 1). In realistic systems, gravitational radiation reaction would provide a dissipation mechanism which would cause a decay of the bars. Using the quadrupole formula

$$\dot{E} \sim \frac{32}{5}\,\Omega_0^6 (I_{xx} - I_{yy})^2 \sim M^2 R^4 \Omega_0^6 \eta^2 \tag{47}$$

(see, e.g., Lai & Shapiro 1995), we can estimate the ratio between the radiation reaction timescale $\tau_{\rm GW}$ and the central rotation period as

$$\frac{\tau_{\rm GW}}{P_c} \sim \frac{1}{\eta^2}\left(\frac{R}{M}\right)^{5/2}\left(\frac{M/R^3}{\Omega_0^2}\right)^{3/2} . \tag{48}$$

Equation (48) implies that as long as the star is not extremely compact, $M/R = O(1)$, the timescale of the radiation reaction is much longer than the dynamical timescale of the system, even if its rotation rate is near break-up, $\Omega_0^2 \sim M/R^3$, and the star is highly deformed, $\eta = O(1)$. In our simulation we choose $M/R \lesssim 0.05$ so that $\tau_{\rm GW}/P_c \gg 1$. Gravitational radiation reaction, which is not present at 1PN order, is therefore irrelevant for the calculations in this paper.

5. CONSERVATION OF CIRCULATION

Considerable effort recently has gone into determining whether or not a bar, once it has saturated, persists for many rotational periods, or whether it decays very soon (see, e.g., New et al. 2000; Brown 2000). Differences in the results are probably because of numerical errors, and possibly caused by the presence of numerical viscosity associated with the finite differencing. In this section we describe how the conservation of circulation in general relativity can be used to check for the presence of numerical viscosity and to establish the reliability of long-time simulations.

According to the Kelvin-Helmholtz theorem, the relativistic circulation,

$$\mathscr{C}(c) = \oint_c h u_\mu \lambda^\mu \, d\sigma , \tag{49}$$

is conserved in isentropic flow along an arbitrary closed curve c (see Carter 1979; Landau & Lifshitz 1982). Here,

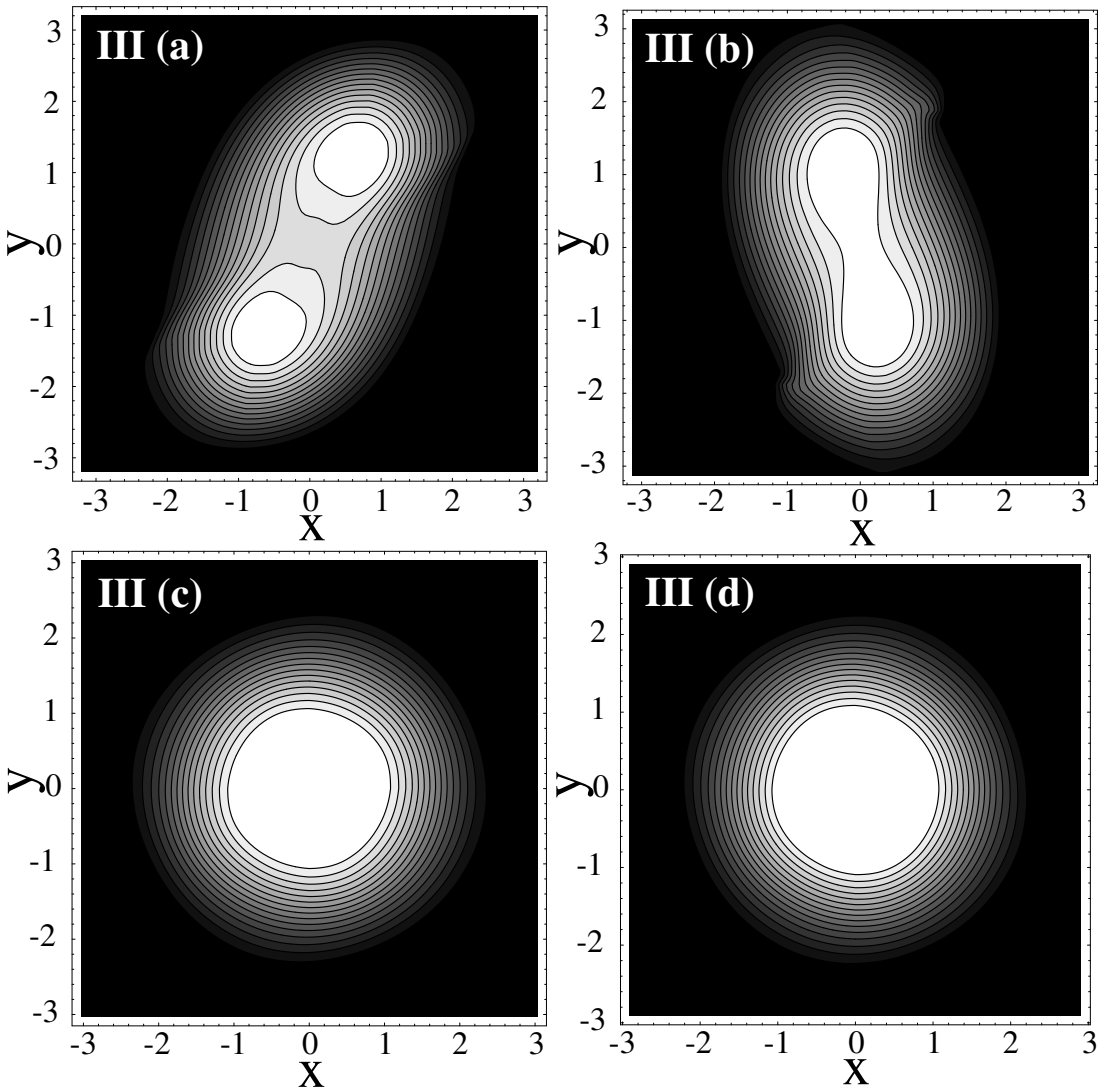

FIG. 6.—Same as Fig. 4, for models III. The contour lines denote densities $\rho_* = 3.1i \times 10^{-4}$ ($i = 1, \ldots, 15$), at times (*a*) $t/P_c = 2.91$, (*b*) $t/P_c = 4.25$, (*c*) $t/P_c = 8.04$, and (*d*) $t/P_c = 7.93$.

$h = 1 + \varepsilon + P/\rho$ is the specific enthalpy, σ is a Lagrange parameter which labels points on the curve c, and λ^μ is the tangent vector to the curve c [i.e., $\lambda^\mu = (\partial/\partial\sigma)^\mu$]. Conservation of C can be verified by computing

$$\begin{aligned}\frac{d}{d\tau}\,C(c) &= \oint_c d\sigma\, u^\nu \nabla_\nu (h u_\mu \lambda^\mu) \\ &= \oint_c d\sigma [\lambda^\mu u^\nu \nabla_\nu (h u_\mu) + (h u_\mu) u^\nu \nabla_\nu \lambda^\mu] \\ &= \oint_c d\sigma [\lambda^\mu u^\nu \nabla_\nu (h u_\mu) + h u_\mu \lambda^\nu \nabla_\nu u^\mu] \\ &= -\oint_c d\sigma\, \lambda^\mu \nabla_\mu h \\ &= 0\,. \end{aligned} \tag{50}$$

Here, to derive the third line from the second line, we use the fact that $u^\mu = (\partial/\partial\tau)^\mu$ and λ^μ are coordinate basis vectors, and thus commute according to

$$u^\mu \nabla_\mu \lambda^\nu = \lambda^\mu \nabla_\mu u^\nu\,. \tag{51}$$

We also have used $u_\mu u^\mu = -1$ and the Euler equation

$$u^\lambda \nabla_\lambda (h u_\mu) = -\nabla_\mu h\,, \tag{52}$$

to obtain the fourth line. Note that it is the derivative of $C(c)$ with respect to the proper time τ that vanishes, so that the circulation has to be evaluated on hypersurfaces of constant proper time as opposed to constant coordinate time.

We check the conservation of circulation for three cases, namely the unstable models I(*b*) and I(*c*), and the stable model I(*d*). For model I(*b*) we evaluate the circulation along three closed curves, and for models I(*c*) and I(*d*) for four. Each loop is located in the equatorial plane, and is initially aligned with a constant density contour. For model I(*b*) we choose loops which intersect $x/r_e = 0.5$, 0.625, and 0.75 on the x axis, and for models I(*c*) and I(*d*) an additional loop which intersects $x/r_e = 0.875$ and $y = 0$. We follow the evolution of each loop with the help of Lagrangian tracers, whose trajectories are computed from

$$\frac{dx^i}{dt} = v^i\,, \quad \frac{d\tau}{dt} = \frac{1}{u^t}\,. \tag{53}$$

The number of test particles representing each loop is 80–140 depending on its initial location. We use a first order

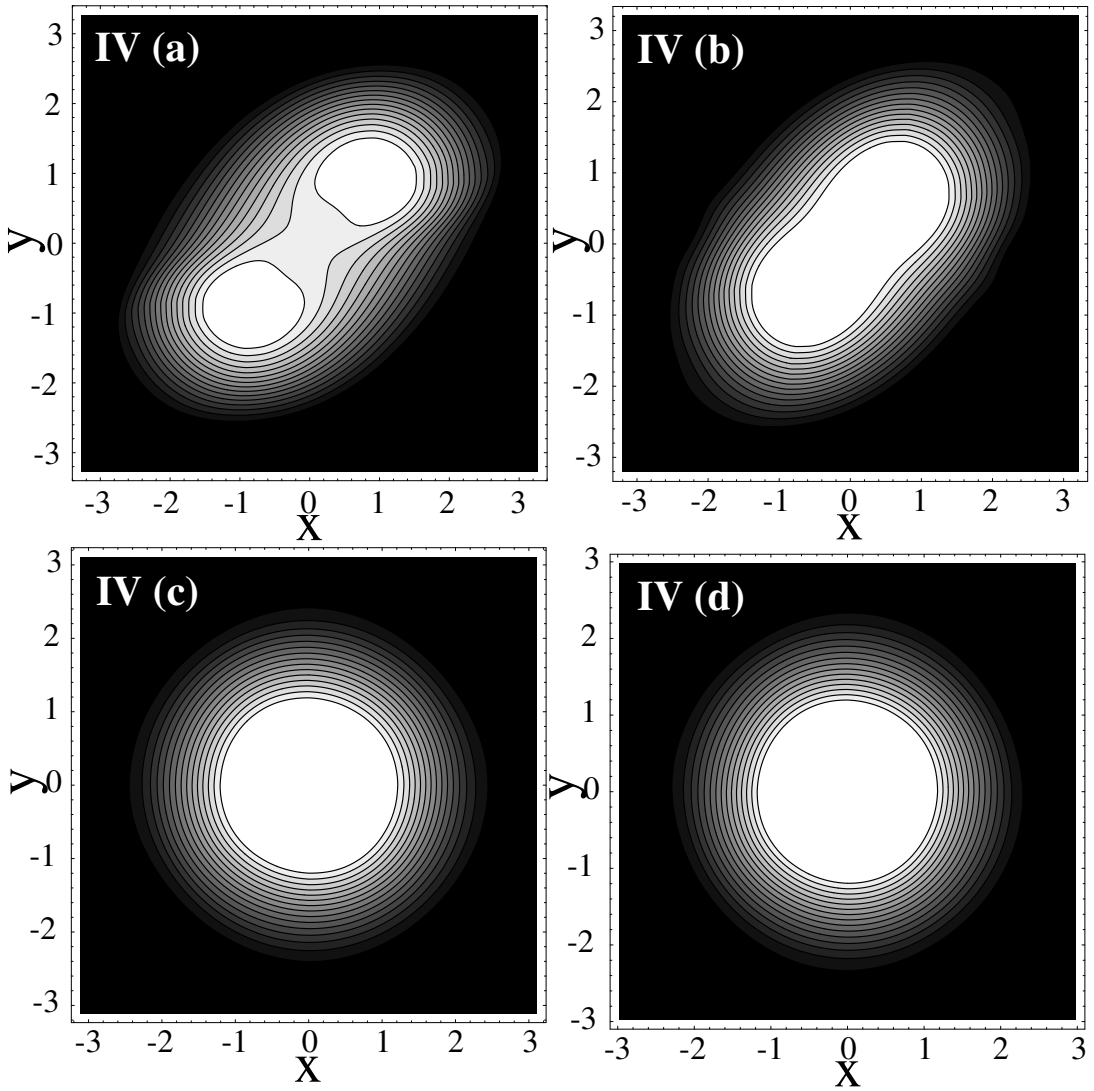

FIG. 7.—Same as Fig. 4, for models IV. The contour lines denote densities $\rho_* = 1.7i \times 10^{-4}$ ($i = 1, \ldots, 14$), at times (*a*) $t/P_c = 2.77$, (*b*) $t/P_c = 7.72$, (*c*) $t/P_c = 9.86$, and (*d*) $t/P_c = 9.73$.

numerical scheme to integrate equation (53) forward in time, once the (Eulerian) hydrodynamic flow has been determined. We evaluate the circulation along a loop c at a proper time τ by interpolating the hydrodynamic variables in both space and time to the current location of the Lagrangian tracers.

TABLE 3

RELATIVE ERROR OF THE CIRCULATION

Model	r/r_e	Initial Value	Final Value	Relative Error (%)
I(*b*).....	0.500	1.198	1.203	0.4
I(*b*).....	0.625	1.651	1.632	1.1
I(*b*).....	0.750	2.053	1.899	7.5
I(*c*).....	0.500	1.173	1.187	1.2
I(*c*).....	0.625	1.603	1.600	0.2
I(*c*).....	0.750	1.989	1.992	0.2
I(*c*).....	0.875	2.330	2.356	1.1
I(*d*).....	0.500	1.129	1.142	1.2
I(*d*).....	0.625	1.535	1.536	0.1
I(*d*).....	0.750	1.903	1.910	0.4
I(*d*).....	0.875	2.228	2.257	1.3

NOTE.—Conservation of circulation for models I(*a*), I(*c*), and I(*d*). We set each of the final circulation value at the endpoint in Fig. 8.

Figure 8 shows that the circulation is well conserved in all three models, indicating that numerical viscosity only has very small effects in our code. In Figure 9 we also show the location of the loops (Lagrangian particles) at the final time steps. As expected, the curves for the dynamically unstable stars (models I[*b*] and I[*c*]) become deformed, while the curves for the dynamically stable star (model I[*d*]) remain close to spherical. The outermost loop in Figure 8 (model I[*b*]) seems to indicate a small violation of the conservation of circulation. However, this loop is close to the surface of a star which forms spiral arms, and is hence strongly deformed (see Fig. 9). The representation of this loop with Lagrangian tracers was therefore not sufficient to accurately evaluate its circulation. We tabulate the relative errors in the circulation in Table 3. Except for the outermost loop in model I(*b*), the circulation is conserved up to $\sim 1\%$ in our simulations.

We would like to emphasize that circulation is conserved in relativity even in the presence of gravitational radiation (as long as the fluid flow is isentropic and no shocks form). As a consequence, conservation of circulation can be used

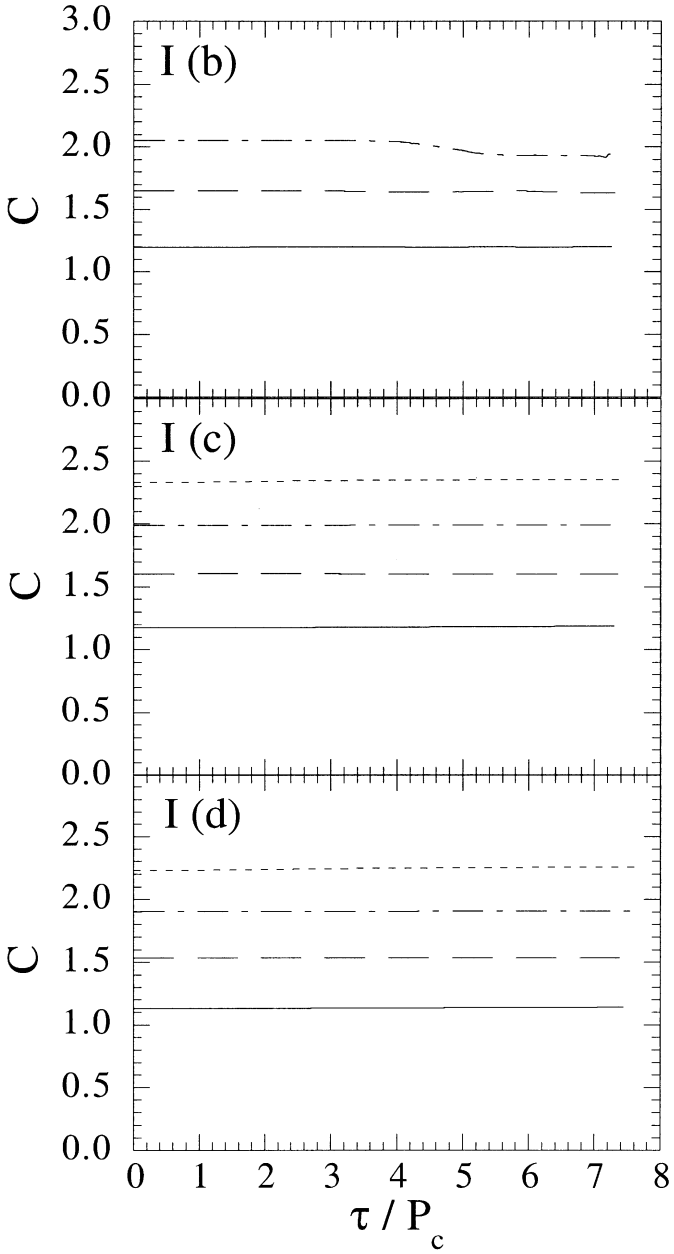

FIG. 8.—Circulation as a function of proper time τ for various loops in models I(*b*), I(*c*), and I(*d*). The loops have an initial radius of $r/r_e = 0.5$ (*solid line*), 0.625 (*dashed line*), 0.75 (*dash-dotted line*), and 0.875 (*dotted line*).

as a very strong code test in fully relativistic simulations as well as Newtonian or post-Newtonian simulations which include gravitational radiation reaction terms.

6. GRAVITATIONAL WAVES

We compute approximate gravitational waveforms by evaluating the quadrupole formula, neglecting all PN corrections. In the radiation zone, gravitational waves can be described by a transverse-traceless, perturbed metric h_{ij}^{TT} with respect to a flat spacetime. In the quadrupole formula, h_{ij}^{TT} can be expressed as (Misner, Thorne, & Wheeler 1973)

$$h_{ij}^{TT} = \frac{2}{r}\frac{d^2}{dt^2}\left(I_{ij}^{TT} - \frac{1}{3}\delta_{ij} I_{kk}^{TT}\right), \tag{54}$$

where r is the distance to the source, and TT denotes the

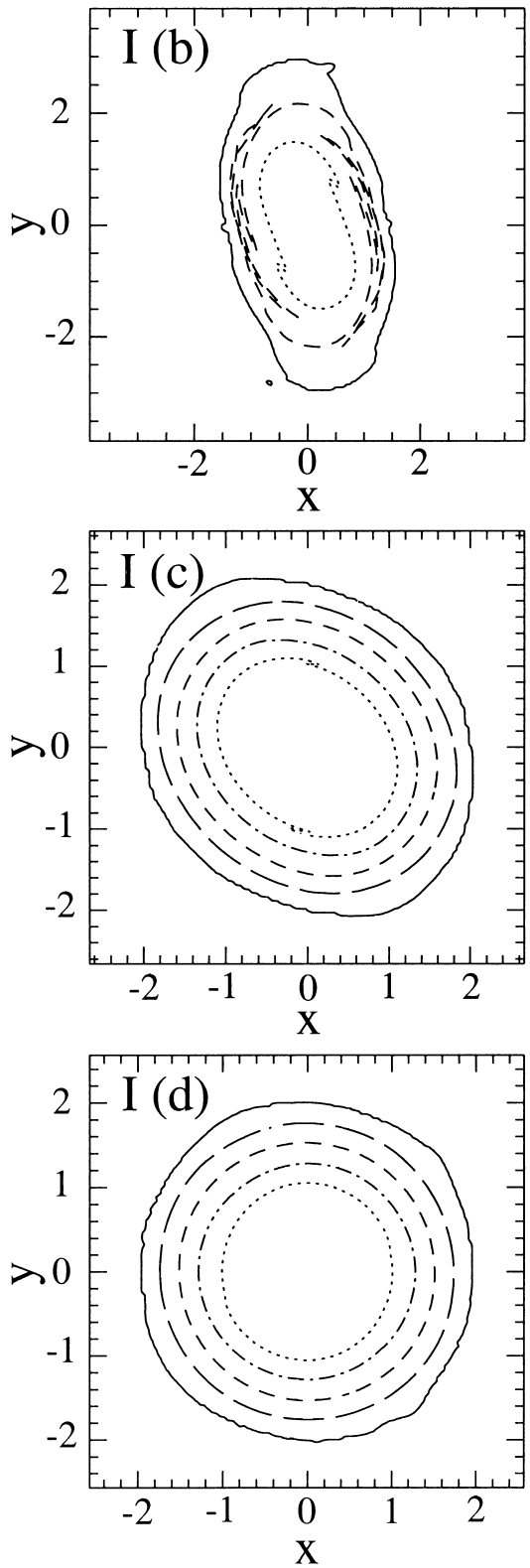

FIG. 9.—Location of Lagrangian test particles at the end of the simulations for model I(*b*) (at $\tau/P_c = 7.37$, 7.26 listed from the outer loop), model I(*c*) (at $\tau/P_c = 11.06$, 10.95, 10.84, 10.75) and model I(*d*) (at $\tau/P_c = 7.67$, 7.59, 7.51, 7.45). Each loop is plotted for a constant value of τ, but different loops correspond to slightly different values of τ. We also include density contours for $\rho_* = 10^{-4}\rho_{*\max}$ (*solid lines*), which nearly coincide with the surface of the star. The long-dashed, dashed, dash-dotted, dotted lines denote the locations of the test particles that are initially located along loops which intersect $x/r_e = 0.875$, 0.750, 0.625, and 0.500 on the x-axis.

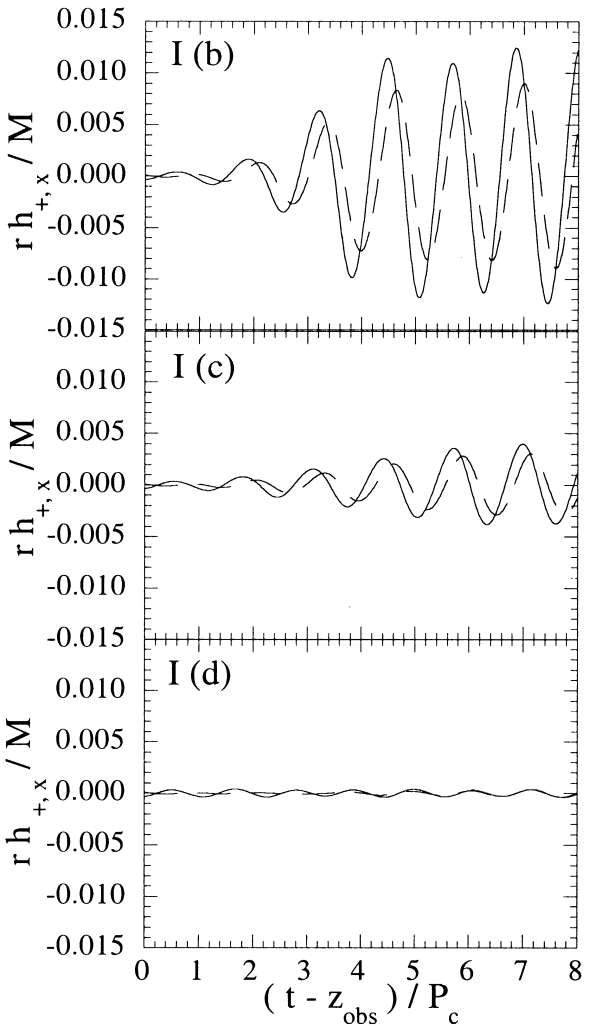

FIG. 10.—Gravitational waveforms rh_+/M (*solid lines*) and $rh_\times/M$ (*dashed lines*) as seen by a distant observer located on the z-axis.

transverse-traceless projection

$$I_{ij}^{TT} = P_i{}^a P_j{}^b I_{ab} - \tfrac{1}{2} P_{ij} P^{ab} I_{ab} , \tag{55}$$

with

$$P_i{}^j = \delta_i{}^j - \hat{n}_i \hat{n}^j , \quad \hat{n}^i = x^i/r . \tag{56}$$

Choosing the direction of the wave propagation to be along the z-axis, the two polarization modes of gravitational waves can be determined from

$$h_+ \equiv \tfrac{1}{2}(h_{xx}^{TT} - h_{yy}^{TT}) , \quad h_\times \equiv h_{xy}^{TT} . \tag{57}$$

Note that this quantity contains second time derivatives of I_{ij}^{TT}, which are difficult to evaluate numerically. We therefore rewrite equation (54) as

$$h_{ij}^{TT} = \frac{2}{r} \frac{d}{dt} \left(\dot{I}_{ij}^{TT} - \frac{1}{3} \delta_{ij} \dot{I}_{kk}^{TT} \right) , \tag{58}$$

and use the continuity equation (eq. [32]) to eliminate the time derivatives in $\dot{I}_{ij}^{TT}$

$$\dot{I}_{ij} = \int (\rho_* v^i x^j + \rho_* x^i v^j) d^3x , \tag{59}$$

(e.g., Finn 1989). We are then left with having to compute only a first time derivative numerically, which can be done much more accurately. For observers along the z-axis, we find

$$\frac{rh_+}{M} = \frac{1}{2M} \frac{d}{dt} (\dot{I}_{xx} - \dot{I}_{yy}) , \tag{60}$$

$$\frac{rh_\times}{M} = \frac{1}{M} \frac{d}{dt} \dot{I}_{xy} . \tag{61}$$

In Figure 10, we plot waveforms for models I(b), I(c), and I(d). For the unstable models I(b) and I(c), we find, as expected, a quasi-periodic oscillation with growing amplitude during the early bar formation. For the stable model I(d), we find a periodic waveform with approximately constant amplitude.

In all three models, the frequency of the periodic oscillations is approximately

$$f \sim \frac{1}{1.3 P_c} \simeq 770 \text{ Hz} \left(\frac{1 \text{ ms}}{P_c} \right) . \tag{62}$$

Once a bar forms and reaches saturation in unstable stars, the oscillation period reduces to slightly smaller values ($\simeq 1.18 P_c$ for model I[b] and $\sim 1.27 P_c$ for model I[c]), and accordingly the frequency shifts to slightly larger values. This shift in the frequency is caused by the significant deformation of the stars by the bars.

The gravitational wave amplitude in model I(b) is approximately

$$h_{\rm GW} \simeq 4.8 \times 10^{-23} \left(\frac{M}{M_\odot} \right) \left(\frac{10 \text{ Mpc}}{r} \right) \left(\frac{rh_{+,\times}/M}{0.01} \right) . \tag{63}$$

Both the frequency and the gravitational wave amplitude are consistent with the fully relativistic results in Shibata et al. (2000).

A detection of these signals by kilometer size laser-interferometric gravitational wave detectors like LIGO (e.g., Thorne 1995) might be feasible, because the waveform is quasi-periodic, which significantly increases its effective amplitude (see Lai & Shapiro 1995). Also, radiation reaction may gradually shift the frequency to smaller values, and hence into a regime where LIGO is more sensitive. The effect of radiation reaction on the evolution of bar modes is not very well understood, though, except in incompressible stars (e.g., Chandrasekhar 1970; Lai & Shapiro 1995) and should be the subject of future studies.

7. SUMMARY

We perform 1PN simulations of rapidly and differentially rotating stars to investigate general relativistic effects on the dynamical bar-mode instability for small compactions $M/R \leq 0.05$. By combining these PN results with the fully relativistic simulations of Shibata et al. (2000) for configurations of higher compaction, we conclude that the critical value of $\beta = \beta_{\rm dyn}$ decreases with increasing M/R. Thus, relativistic gravitation enhances the bar-mode instability.

We also describe how conservation of circulation can be used to check by how much a code is affected by numerical viscoscity. In the presence of significant numerical viscosity, long-time evolution calculations become very unreliable and may lead, for example, to erroneous evolution of a saturated bar. We show that in our calculations the circulation is well conserved, implying that our code is at most very weakly affected by numerical viscosity. We present a method for computing the circulation which can be applied in Newtonian, post-Newtonian, and fully relativistic calculations.

This work was supported by JSPS Grant-in-Aid 5689, NSF grants AST 96-18524 and PHY 99-02833, and NASA grant NAG5-7152 at the University of Illinois at Urbana-Champaign. M. Shibata gratefully acknowledges support by JSPS (Fellowships for Research Abroad) and the hospitality of the Department of Physics at UIUC; T. W. Baumgarte is pleased to acknowledge support through a Fortner Fellowship. Numerical computations were performed on the VX/4R machines in the Astronomical Data Analysis Center of the National Astronomical Observatory of Japan, and on the FUJITSU-VX/S vector computer at Media Network Center, Waseda University.

REFERENCES

Baumgarte, T. W., & Shapiro, S. L. 1999, Phys. Rev. D, 59, 024007
Blanchet, L., Damour, T., & Schäfer, G. 1990, MNRAS, 242, 289
Bonazzola, S., Frieben, J., & Gourgoulhon, E. 1996, ApJ, 460, 379
———. 1998, A&A, 331, 280
Bonazzola, S., Gourgoulhon, E., Salgado, M., & Marck, J. A. 1993, A&A, 278, 421
Bowen, J. M., & York, Jr., J. W. 1980, Phys. Rev. D, 21, 2047
Brown, J. D. 2000, Phys. Rev. D, 62, 084024
Carter, B. 1979, in Active Galactic Nuclei, ed. C. Hazard & S. Mitton (Cambridge: Cambridge Univ. Pres), 273
Chandrasekhar, S. 1965, ApJ, 142, 1488
———. 1969, Ellipsoidal Figures of Equilibrium (New York: Yale Univ. Press), 61
———. 1970, ApJ, 161, 561
Cook, G. B., Shapiro S. L., & Teukolsky, S. A. 1992, ApJ, 398, 203
———. 1994, ApJ, 422, 227
Cutler, C., & Lindblom, L. 1992, ApJ, 385, 630
Durisen, R. H., Gingold, R. A., Tohline, J. E., & Boss, A. P. 1986, ApJ, 305, 281
Finn, L. S. 1989, in Frontiers in Numerical Relativity, ed. C. R. Evans, L. S. Finn, & D. W. Hobill (Cambridge: Cambridge Univ. Press), 126
Friedman, J. L., & Schutz, B. F. 1978, ApJ, 222, 281
Houser, J. L., & Centrella, J. M. 1996, Phys. Rev. D, 54, 7278
Houser, J. L., Centrella, J. M., & Smith, S. C. 1994, Phys. Rev. Lett., 72, 1314
Imamura, J. N., Toman, J., Durisen, R. H., Pickett, B. K., & Yang, S. 1995, ApJ, 444, 363
Ipser, J. R., & Lindblom, L. 1990, ApJ, 355, 226
Komatsu, H., Eriguchi, Y., & Hachisu, I. 1989, MNRAS, 237, 355
———. 1989b, MNRAS, 239, 153
Lai, D., & Shapiro, S. L. 1995, ApJ, 442, 259
Landau, L. D., & Lifshitz, E. M. 1982, Fluid Mechanics (2d ed.; Oxford: Pergamon)
Lynden-Bell, D., & Ostriker, J. P. 1967, MNRAS, 136, 293
Misner, C. W., Thorne, K. S., & Wheeler, J. A. 1973, Gravitation (New York: Freeman), 996
New, K. C. B., Centrella, J. M., & Tohline, J. E. 2000, Phys. Rev. D, 62, 064019
Ostriker, J. P., & Bodenheimer, P. 1973, ApJ, 180, 171
Pickett, B. K., Durisen, R. H., & Davis, G. A. 1996, ApJ, 458, 714
Salgado, M., Bonazzola, S., Gourgoulhon, E., & Haensel, P. 1994, A&A, 291, 155
Shapiro, S. L., & Teukolsky, S. A. 1983, Black Holes, White Dwarfs, and Neutron Stars (New York: Wiley)
Shapiro, S. L., & Zane, S. 1998, ApJS, 117, 531
Shibata, M. 1999a, Phys. Rev. D, 60, 104052
———. 1999b, Prog. Theor. Phys., 101, 1199
Shibata, M., Baumgarte, T. W., & Shapiro, S. L. 1998, Phys. Rev. D, 58, 23002
———. 2000, ApJ, 542, 453
Shibata, M., & Nakamura, T. 1995, Phys. Rev. D, 52, 5428
Smith, S. C., Houser, J. L., & Centrella, J. M. 1996, ApJ, 458, 236
Stergioulas, N., & Friedman, J. L. 1998, ApJ, 492, 301
Tassoul, J. 1978, Theory of Rotating Stars (Princeton: Princeton Univ. Press)
Thorne, K. S. 1995, in Proceeding of Snowman 95 Summer Study on Particle and Nuclear Astrophysics and Cosmology, ed E. W. Kolb & R. Peccei (Singapore: World Scientific), 398
Tohline, J. E., Durisen, R. H., & McCollough, M. 1985, ApJ, 298, 220
Tohline, J. E., & Hachisu, I. 1990, ApJ, 361, 394
Toman, J., Imamura, J. N., Pickett, B. J., & Durisen, R. H. 1998, ApJ, 497, 370
Williams, H. A., & Tohline, J. E. 1988, ApJ, 334, 449
Yoshida, S., & Eriguchi, Y. 1999, ApJ, 515, 414